Polymer Chemistry

PAPER

View Article Online
View Journal | View Issue

Cite this: *Polym. Chem.*, 2014, **5**, 771

Polymer bottlebrushes with a redox responsive backbone feel the heat: synthesis and characterization of dual responsive poly(ferrocenylsilane)s with PNIPAM side chains†

Edit Kutnyánszky, Mark A. Hempenius and G. Julius Vancso*

Received 13th August 2013
Accepted 8th September 2013

DOI: 10.1039/c3py01095c

www.rsc.org/polymers

Molecular bottlebrushes, possessing a redox-responsive poly(ferrocenylsilane) (PFS) backbone and temperature-responsive poly(*N*-isopropylacrylamide) (**PNIPAM**) side chains, distributed homogeneously or as a gradient along the PFS main chain, were synthesized. Attachment of the **PNIPAM** chains *via* azide–alkyne click chemistry, or grafting from a PFS macroinitiator backbone by ATRP, resulted in cylindrical shaped molecular bottlebrushes. We found the bottlebrushes to be both redox and temperature responsive, with little influence of one responsiveness on the other. In an aqueous environment above 32 °C the bottlebrushes collapsed to 70% of their original size due to the temperature sensitive side chains, and reversibly recovered their initial size upon cooling as revealed by Dynamic Light Scattering (DLS). Cyclic voltammograms showed electrochemical behavior typical of well solvated, single PFS chains. The backbone of the deposited molecules was in close proximity to the highly ordered pyrolytic graphite (HOPG) electrode surface and was accessible to the supporting electrolyte owing to the presence of the hydrophilic **PNIPAM** side chains. The bottlebrush molecules were deposited on HOPG surfaces for direct molecular visualization by atomic force microscopy (AFM). Molecular size data obtained by DLS and AFM showed good agreement. The bottlebrushes, reported here, are excellent candidates as addressable components for future devices *e.g.* to carry and deliver molecular payloads.

1 Introduction

Stimuli-responsive macromolecular bottlebrushes exhibit reversible changes in their shape, size and various properties when triggered by variations in pH,[1,2] temperature,[3,4] and magnetic field strength or by irradiation with light,[5] which enables their use in areas such as actuation,[6] controlled drug delivery[7,8] and many others.[9] Responsiveness of bottlebrush polymers to these classical stimuli is well documented in the literature. Redox stimuli, which can be applied locally and may be controlled externally, however, are virtually unexplored as means to address molecular bottlebrushes. From a structural point of view, macromolecular bottlebrushes are polymer architectures, constructed from a backbone and polymer side chains, connected to the repeat units of the backbone.[10–12] Due to steric hindrance between the side chains, bottlebrushes adopt an extended, cylindrical conformation. Compositional diversity of bottlebrush polymers has increased in recent years, leading to random, block or gradient copolymer main chains[13] and side chains. The construction of bottlebrushes from both stimuli responsive backbones and side chains opens up new application opportunities in various fields and is expected to yield novel, fascinating and addressable materials.[14–16] Interestingly, the majority of stimuli responsive bottlebrushes are obtained by atom transfer radical polymerization[17,18] (ATRP) "grafting from" processes from poly(2-bromoisobutryloxyethyl methacrylate) (PBIEM) backbones, therefore displaying only side chain stimuli responsiveness. In the few examples of dual responsive systems, responses to one environmental change enhanced changes induced by other stimuli,[7,9,14–16] for instance causing emphasized collapse of the molecules as a result of increased intra- or intermolecular interactions. Responsiveness to multiple stimuli can be achieved in molecular brushes by attaching polymer side chains that differ from the backbone[7,14] or by connecting block copolymers as side chains, leading to core–shell bottlebrushes.[14]

Synthesis of defined molecular bottlebrushes requires the growth of polymer chains with a controlled degree of polymerization. A polymer backbone with reactive pendant groups that can initiate chain growth is required for bottlebrush construction using the "grafting from" method. Alternatively, bottlebrushes are obtained from backbones possessing pendant moieties that allow attachment of pre-formed, end-reactive

Materials Science and Technology of Polymers, MESA+ Institute for Nanotechnology, University of Twente, P.O. Box 217, 7500 AE Enschede, The Netherlands. E-mail: g.j.vancso@utwente.nl; Fax: +31 53 489 3823; Tel: +31 53 489 2974

† Electronic supplementary information (ESI) available. See DOI: 10.1039/c3py01095c

chains in a "grafting to" process.[19,20] Although grafting densities achieved by employing the "grafting to" method are limited for steric reasons, the method remains attractive as side chains of defined degrees of polymerization can be prepared and characterized thoroughly before their attachment to the bottlebrush main chain. The development of efficient coupling methods such as the Cu(I) catalyzed Huisgen cycloaddition between an azide and an alkyne group has helped to increase grafting densities in "grafting to" processes and therefore has increased the viability of this approach.[21–25]

Here we discuss macromolecular architectures based on a poly(ferrocenylsilane) (PFS) main chain and poly(*N*-isopropylacrylamide) (**PNIPAM**) side chains, distributed either homogeneously or as a gradient along the PFS backbone. These structures are expected to expand or contract in response to external stimuli. The bottlebrushes can be triggered through oxidation–reduction cycles involving the PFS main chain[26,27] or by temperature changes to which **PNIPAM** side chains respond in an aqueous environment. As discovered by the Manners group, PFSs are accessible by thermal, anionic and transition metal-catalyzed ring-opening polymerization (ROP) of [**1**]silaferrocenophanes,[28–31] driven by the significant ring strain present in these cyclic monomers. Recently, the Manners group described photoassisted living anionic ring opening polymerization, requiring milder initiators and thereby broadening the range of anionically polymerizable silaferrocenophane monomers.[32] Here we chose to use platinum-catalyzed ROP as this leads to high molar mass PFSs, is compatible with our functional side groups[30,33–39] and allows the copolymerization of strained cyclic silanes. By the continuous introduction of silaferrocenophane A into a polymerizing mixture of silaferrocenophanes A and B, a gradual decrease in the concentration of B is expected to result as chain growth progresses, producing gradient copolymers.[40–44]

PNIPAM is one of the most commonly used polymers for the preparation of temperature responsive bottlebrushes,[12] since it can be obtained by controlled radical methods such as reversible addition-fragmentation chain transfer (RAFT) polymerization,[45–47] or ATRP.[48–50] In aqueous solutions, **PNIPAM** exhibits a lower critical solution temperature (LCST) around 32 °C.[51] Upon heating, the homogeneous polymer solution becomes turbid and the polymer precipitates. The LCST of **PNIPAM** can be influenced/shifted by the solution composition,[10,52] by copolymerization with other monomers[45,53–55] and by the end group.[56]

Molecular bottlebrushes, reported here, were prepared using "grafting to" and "grafting from" processes. The "grafting to" method involves a click reaction between an azide functionalized PFS backbone and alkyne end-functionalized **PNIPAM** chains. In the "grafting from" method, ATRP initiator moieties are connected as side groups to the PFS backbone to form an organometallic macroinitiator. The gradient bottlebrushes targeted here possess a gradient in hydrophilicity along their backbone which is of interest for their organization on surfaces and for inducing directed molecular motion, triggered by stimuli.

2 Results and discussion

A generic method for obtaining PFS chains with pendant functional groups involves the ring-opening polymerization of [**1**](3-chloropropyl)methylsilaferrocenophane **SF-Cl** to poly(ferrocenyl(3-chloropropyl)methylsilane) **1**, which can be derivatized further by nucleophilic substitution reactions.[37] For instance, it can be converted into its more reactive iodo analogue, poly(ferrocenyl(3-iodopropyl)methylsilane) **2**, allowing a wider

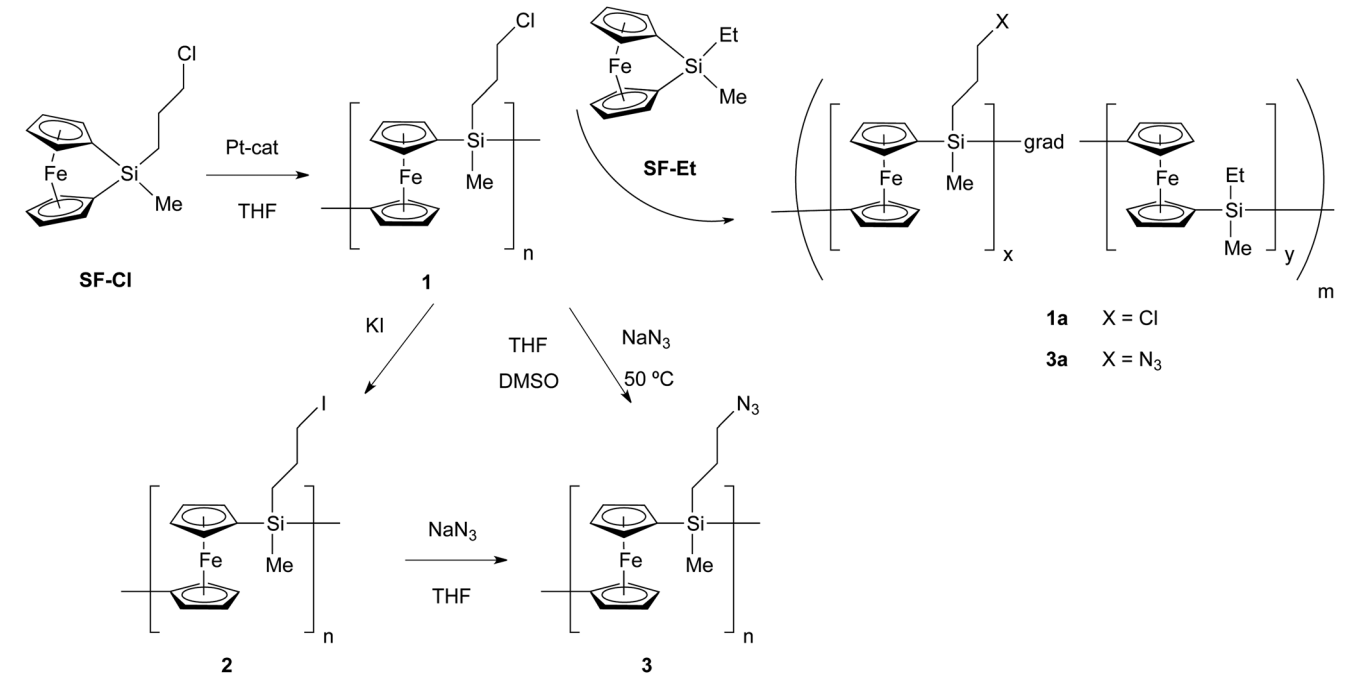

Scheme 1 Azide functionalization of the PFS homopolymer and the structure of azide modified gradient PFS **3a**.

Table 1 Molar mass characteristics of the gradient PFSs

	M_n[a] 10^3 g mol^{-1}	M_w 10^3 g mol^{-1}	$Đ$	M_w[b] 10^3 g mol^{-1}
S1	99.2	181	1.80	181
S2	126	287	2.25	211
S3	131	302	2.30	221
1a	142	376	2.65	248

[a] Measured in THF against narrow $Đ$ polystyrene standards. [b] Peak molar mass.

range of functional moieties to be attached in subsequent side group conversion reactions. PFS homopolymers **1** and **2**, with various degrees of polymerization, were synthesized (Scheme 1).

To obtain PFS chains with a gradient in composition, two different silaferrocenophane monomers were copolymerized: **SF-Cl** and [**1**]ethylmethylsilaferrocenophane **SF-Et**. As [**1**]silaferrocenophanes can be copolymerized with other strained, cyclic alkylsilanes in the presence of platinum catalysts,[30] copolymers of [**1**]silaferrocenophanes are likely formed by ring opening polymerization. A stepwise decrease in the concentration ratio [**SF-Cl**]/[**SF-Et**] was achieved by controlling the monomer feed. Sequential introduction of the monomers to the polymerization solution resulted in poly(ferrocenyl(3-chloropropyl)methylsilane)-*grad*-poly(ferrocenylethylmethylsilane) **1a** (Scheme 1).

The Pt-catalyzed ring opening polymerization was started with **SF-Cl**, forming a pure **SF-Cl** block. Polymerization was allowed to proceed for 1 h, a sample **S1** was taken for analysis and then the **SF-Et** monomer was introduced. After another hour another sample was taken (**S2**) and again **SF-Et** was added to the solution. After 1 h a third sample was taken (**S3**) and **SF-Cl** was added. The polymerization was continued for another 5 h to obtain the gradient polymer (**1a**). Each sample and also the final product were precipitated in methanol. The samples were characterized by means of ^{1}H NMR spectroscopy and GPC to gauge the progress of the polymerization.

^{1}H NMR spectra recorded from each sample (Fig. S5, ESI†) show how the polymer composition evolves with the proceeding reaction. The chemical shift of the signal belonging to the methyl group at the silicon atom differs for the two different repeat units. Therefore, the integral ratio of these two singlets provides information about the composition of the polymer. **S1** only contained **SF-Cl** units which feature a Si–CH_3 peak at $\delta = 0.52$ ppm. Since **SF-Cl** was gradually replaced by **SF-Et**, the relative number of incorporated **SF-Cl** units decayed, as was evident from the temporal sampling. The final product **1a** possessed around 35% **SF-Cl** and 65% **SF-Et** units, which is in agreement with the feed ratio. To ensure that polymerization proceeded during the course of the experiment, GPC measurements were carried out for each sample (Fig. S6, ESI†). The obtained traces show a monomodal distribution and a peak maximum that shifted to lower elution volumes from **S1** to the final product. The polystyrene-effective molar masses and polydispersities obtained for the samples are summarized in Table 1. The relative increase in the molar mass lessens, showing that the polymerization rate decreases with time, likely due to a higher viscosity caused by the growing polymer. The polydispersity ($Đ$) of the samples increased from 1.82 to 2.65, which are typical values for PFSs obtained by Pt-catalyzed ring-opening polymerization.

To obtain molecular bottlebrushes, PFS backbones were functionalized with pendant azide groups for use in the azide–alkyne Huisgen cycloaddition (click reaction). Both **1** and **2** were reacted with NaN_3, yielding poly(ferrocenyl(3-azidopropyl)-methylsilane) **3**.[57] Similarly, the reaction of **1a** and NaN_3 yielded poly(ferrocenyl(3-azidopropyl)methylsilane)-*grad*-poly-(ferrocenylethylmethylsilane) **3a** (Scheme 1). ^{1}H NMR spectroscopy showed that the signal belonging to 3-CH_2, directly adjacent to Cl, I or N_3 (Fig. S1 and S7, ESI†), shifted to a new position following each derivatization. Clearly, near-quantitative side group conversion was achieved in each reaction. This was further evidenced by ^{13}C NMR spectroscopy, showing the expected chemical shifts and a complete disappearance of starting material peaks. Complete substitution in the case of **2** was achieved at room temperature in tetrahydrofuran, while **1**

Table 2 Molar mass characteristics of bottlebrush building blocks

Polymer	$M_{n,NMR}$[a] 10^3 g mol^{-1}	$M_{n,GPC}$ 10^3 g mol^{-1}	$M_{w,GPC}$ 10^3 g mol^{-1}	$Đ$	$DP_{n,GPC}$	$DP_{n,NMR}$
$\mathbf{2}_{373k}$[e]	n.a	169[b]	373	2.20	429	
$\mathbf{3}_{373k}$	n.a	112[b]	227	2.02	429	
$\mathbf{1}_{284k}$	n.a	94[b]	284	3.00	303	
$\mathbf{3}_{284k}$	n.a	46[b]	347	7.60	303	
$\mathbf{1}_{595k}$	n.a	302[b]	595	1.95	965	
$\mathbf{3}_{595k}$	n.a	61[b]	294	4.80	965	
1a	n.a	142	376	2.65	n.a	
3a	n.a	37[b]	115	3.15	n.a	
5[d]	n.a	41[a]	91	2.20	n.a	
$\mathbf{PNIPAM}_{13k}$	11	12[c]	13	1.1	104	93
$\mathbf{PNIPAM}_{30k}$	19	26[c]	30	1.15	233	168
$\mathbf{PNIPAM}_{7k}$	6	6[b]	7	1.15	56	56

[a] Obtained from ^{1}H NMR, based on alkyne–CH_2 and **PNIPAM** repeat unit integral values. [b] Measured in THF against narrow polystyrene standards. [c] Measured in 0.1 M LiCl/DMF against well-defined poly(methyl methacrylate) standards. [d] Precursor $\mathbf{1}_{284k}$. [e] Subscripts denote polymer M_w (g mol^{-1}).

required the presence of a polar aprotic solvent (DMSO) and moderate heating to fully convert into **3**. ^{1}H NMR spectroscopy also indicated a quantitative conversion of **1a** to **3a**.

For defined molecular bottlebrushes, side group interconversions must proceed quantitatively and the backbone must remain intact during these steps. To ensure the absence of chain scission, gel permeation chromatography (GPC) measurements were performed (Fig. S2 and S8, ESI†). The shapes of the peaks were similar, but the peak of **3** had shifted to a higher elution volume with respect to the signal of **1**, suggesting a lower molar mass for **3**. However, as the polydispersities are similar and no obvious signals belonging to low molar mass polymer chains were present, chain scission can be ruled out. The lower polystyrene-effective molar mass of **3** compared to **1** most likely is caused by a smaller hydrodynamic volume of coil **3** due to dipolar intramolecular interactions between its azide moieties. Polystyrene-effective molar masses and polydispersities of these polymers are summarized in Table 2.

PNIPAM side chains suitable for "grafting to" assembly of bottlebrushes were synthesized by RAFT and ATRP processes, using alkyne-functional initiators. In the case of RAFT, *S*-1-dodecyl-*S*′-(α,α′-dimethyl-α′′-propargyl acetate) was used as a chain transfer agent.[58] This process was conducted according to a literature procedure where the CTA concentration was adjusted to control the molar mass (Table 2 and Scheme 2). ATRP polymerization of NIPAM was carried out in a DMF/2-propanol mixture, using 3-(trimethylsilyl)prop-2-yn-1-yl-2-chloropropanoate as an initiator.[59]

2.1 Synthesis of molecular bottlebrushes *via* a "grafting to" method

The click reaction by which the **PNIPAM** chains are attached to the PFS backbone (Scheme 2) was conducted in THF in the presence of a Cu^0/Cu^I catalyst system, formed *in situ* by reduction of Cu^{II} to Cu^0 with sodium ascorbate.[24] After this grafting step, the reduced Cu was removed by centrifugation. Subsequently, the unreacted **PNIPAM** chains were removed by dialysis, using large-pore dialysis tubing. The solubility of the dark yellow-amber product in water already gave an indication of the successful **PNIPAM** attachment to the hydrophobic PFS backbone. Interestingly, when 5% DMSO was added to the reaction mixture, the click reaction proceeded faster. Bottlebrushes **Bb1**, **Bb2**, **Bb3** and **grBb** were obtained by attaching $\mathbf{PNIPAM}_{13k}$ to $\mathbf{3}_{373k}$, $\mathbf{PNIPAM}_{30k}$ to $\mathbf{3}_{284k}$, $\mathbf{PNIPAM}_{7k}$ to $\mathbf{3}_{595k}$ and $\mathbf{PNIPAM}_{30k}$ to **3a**, respectively. In the case of **Bb3** and **grBb** the reaction resulted in a highly viscous material with good solubility in methanol. In water both showed swelling but even upon vigorous shaking they did not dissolve fully. This behavior is due to hydrophobic interactions of the *n*-dodecyl groups present at the **PNIPAM** chain ends, originating from the RAFT initiator. In the case of **grBb** the hydrophobic PFS tail contributes to these interactions. To overcome this problem, the dodecyl groups were cleaved by addition of 1-hexylamine (Fig. 1). To avoid disulfide formation, the produced thiol groups were protected with the NIPAM monomer attached *via* a thiol-ene addition reaction.[60] The obtained products showed a high solubility in water.

First, the molecular bottlebrushes were characterized by ATR-FTIR spectroscopy. For all bottlebrushes, ATR-FTIR spectra (Fig. S4 and S9, ESI†) clearly show, besides the characteristic peaks of **PNIPAM** at 1635 and 1535 cm^{-1} of the amide group, a characteristic peak at 1036 cm^{-1}, belonging to the out-of-plane vibration of the ferrocene rings.[61] Compared to other PFS–**PNIPAM** composite structures in the literature[62] possessing a few wt% PFS in **PNIPAM**, relative signal intensities of the ferrocene out-of-plane vibration and the **PNIPAM** carbonyl

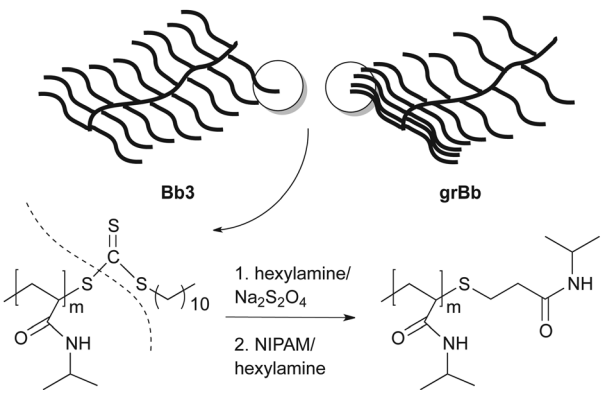

Fig. 1 Dodecyl end group removal for **PNIPAM** chains of bottlebrushes **Bb3** and **grBb**.

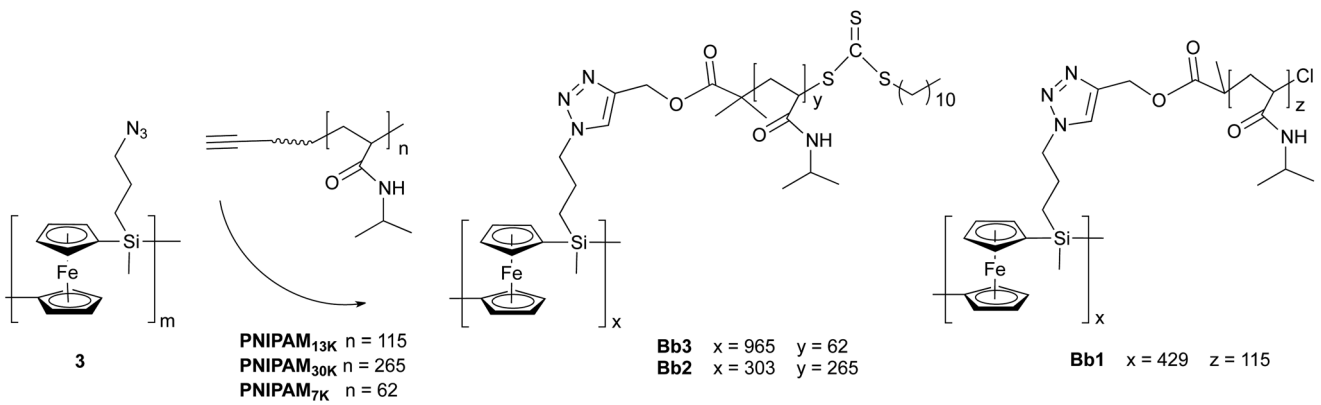

Scheme 2 Cycloaddition click reaction between an azide functional PFS backbone and alkyne end-functional **PNIPAM** chains.

stretch at 1635 cm^{-1} in the FTIR spectra suggest that the bottlebrushes contain around 1–5% PFS. Importantly, the absence of the azide stretching peak at 2088 cm^{-1} in all bottlebrush spectra provides evidence for completion of the click reaction. Considering that this absorption appears as a strong signal in the spectrum of **3**, one may conclude that the efficiency of the grafting reaction and therefore the obtained grafting densities are high. The gradient bottlebrush shows a higher PFS content than the previously made, homogeneous bottlebrushes.

Even though the number of **PNIPAM** repeat units clearly outweighs the number of PFS repeat units, signals of both are present in the ^{1}H NMR spectra of the bottlebrushes. On the basis of M_n values of the backbone, and the ratio of the repeat units of the backbone and the side chains, one may estimate the molar mass of the bottlebrush molecules. In principle, one might estimate the grafting density (Γ) by comparing actual ^{1}H NMR integral ratios of the PFS and **PNIPAM** repeat units with ratios for fully grafted bottlebrushes. The theoretical and estimated molar masses resulting from this are given in Table 3. Since the effective fractionation range of our GPC columns extends to around 2 million g mol^{-1}, the gradient bottlebrush was not analyzed by GPC. Gel permeation chromatography and thermogravimetric analysis of the bottlebrushes are summarized in the ESI.†

2.2 Synthesis of molecular bottlebrushes *via* a "grafting from" method

Bottlebrushes were also grown *via* a "grafting from" process. Poly(ferrocenyl(3-aminopropyl)methylsilane) **4** (ref. 33 and 63) was synthesised according to the literature starting from $\mathbf{1}_{284}$ (for details see Scheme S3, ESI†). **4** was treated with 2-chloropropionyl chloride to introduce pendant ATRP initiator groups, resulting in macroinitiator **5** (Scheme 3). ^{1}H NMR spectroscopy (Fig. S11a, ESI†) showed the formation of an amide bond as was evident from the appearance of an N–H signal at $\delta = 6.6$ ppm. Furthermore, characteristic peaks at $\delta =$ 1.8 and 4.4 ppm, belonging to the 2-chloropropionate moiety, were present in the spectrum. ^{13}C NMR measurements confirmed the full conversion of **4** into **5**. The completion of the reaction was further supported by FTIR spectroscopy by the appearance of the characteristic amide peaks. The new absorption peaks, amide I, N–H symmetrical–asymmetrical stretching vibration at 3290 cm^{-1}, the C═O stretching vibration at 1655 and amide II at 1528 cm^{-1}, are present in the spectrum and well-separated from other clearly resolved vibrational and stretching absorption peaks (Fig. S11b, ESI†).

PNIPAM chains were grown from PFS macroinitiator **5** by means of ARGET-ATRP (continuously regenerated by electron transfer ATRP),[64] producing bottlebrush **Bb4**. The reaction was conducted in a THF–DMF mixture in the presence of ascorbic acid as the *in situ* reducing agent. Molar mass characteristics of the obtained bottlebrush molecule are given in Table 3. Signals of both the **PNIPAM** repeat units and the PFS repeat units were present in the ^{1}H NMR spectrum. Based on the M_n values of the backbone, estimation of the side chain length as well as of the molar mass of the bottlebrush molecules could be made. This approach does not provide information on the actual grafting density of the **PNIPAM** side chains. Resolving the grafting density in these branched structures is a complex issue.[65] The GPC trace of **Bb4** (Fig. S10, ESI†) shows a signal at a low elution volume, indicative of a high molar mass product. This GPC trace is very similar to that of the "grafting to" product **Bb1**, displayed in Fig. S3 (ESI).†

2.3 AFM investigation

Following the molecular characterization of bottlebrush molecules by NMR, GPC and FTIR, atomic force microscopy (AFM) measurements were carried out which provide information on the topology of the synthesized architectures. In the case of successful "grafting to" reactions, but especially "grafting from" reactions, high grafting densities can be expected which directly influence the stiffness of the bottlebrushes and thereby their molecular shape. AFM measurements were carried out in the

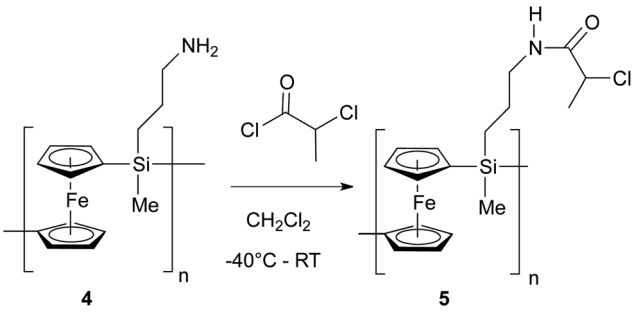

Scheme 3 Coupling of ATRP initiator moieties with aminopropyl-functional PFS.

Table 3 Molar mass characteristics of bottlebrush polymers

	$M_{n,GPC}$[a] $\times 10^6$ g mol^{-1}	$M_{w,GPC}$ 10^6 g mol^{-1}	$Đ$	**PNIPAM** $DP_{n,NMR}$[b]	**PNIPAM** $M_{n,NMR}$[b] 10^3 g mol^{-1}	$M_{n,calc}$ 10^6 g mol^{-1}	Γ chains/ repeat unit
Bb1	2.143	2.519	1.18	38	4.3	1.986	0.41
Bb2				133	15.0	4.613	0.75
Bb3				42	4.7	4.835	0.78
Bb4	2395	2882	1.20	22	2.4	869	n.a
grBb				133	15	2.692	0.78

[a] Measured in THF against narrow polystyrene standards. [b] Obtained from ^{1}H NMR, based on PFS (Si–CH_3) and **PNIPAM** repeat unit integral values.

dry state. Fig. 2 shows topographic images of the bottlebrushes deposited on a highly ordered pyrolytic graphite (HOPG) surface from acetone solution. In most cases curved, cylindrical shaped molecules were observed with various lengths ranging from 30–100 nm for the different samples. In Table 4 the average contour lengths (L_c) of the molecules are presented. Each bottlebrush molecule was deposited on several substrates and for each deposition, three to four images were captured. The height and the width of the molecules ranged from 1.8–2.5 and 11–18 nm, respectively. In the case of **grBb** molecules, structures ranging from 30 nm to 200 nm were found, indicating the presence of aggregated molecules, formed by association of the hydrophobic PFS tail in aqueous solution. This finding is supported by DLS measurements (see later).

2.4 Temperature responsiveness of the bottlebrushes

Light scattering measurements constitute a powerful method for acquiring the average diameter of the synthesized bottlebrush molecules in water, *i.e.* in their solvated state. By performing the measurements as a function of temperature, dimensional changes induced by temperature variation can be monitored directly. Dynamic light scattering (DLS) measurements were carried out in aqueous solution at concentrations of around 0.5 w/w%. A laser with a wavelength $\lambda = 534$ nm was used and the solution temperature was controlled within ± 0.1 °C. From the obtained auto-correlation function of the scattered light the average hydrodynamic radius (R_h) of the molecular bottlebrush molecules was calculated.

Table 4 Average contour lengths of the bottlebrushes, determined from the AFM images

	L_c (nm)
Bb1	36 ± 9
Bb2	47 ± 14
Bb3	35 ± 12
Bb4	65 ± 17

Temperature scans were carried out by increasing/lowering the temperature stepwise with increments of 1–3 °C. For **Bb1**, **Bb3** and **Bb4**, R_h decreased with increasing temperature and increased with decreasing temperature, while **Bb2** showed an increase in size upon heating above 32 °C and a decrease upon cooling. The initial size of the macromolecules was reversibly regained in every case upon cooling (Fig. 3). The LCST temperature was determined from the graphs to be around 32 °C, since this was the temperature at which the scattering intensity increased sharply, indicating structural changes in the bottlebrush molecules resulting from **PNIPAM** collapse.[66] The size of **Bb1**, **Bb3** and **Bb4** continued to decrease above the LCST temperature as a result of intramolecular collapse, while **Bb2** bottlebrushes aggregated above this temperature. The size reductions displayed by bottlebrushes upon crossing the LCST were from 33 to 20 nm (61%) for **Bb1**, and from 35 to 20 nm (57%) for **Bb3**, while **Bb4** contracted from 105 to 80 nm (76%) and **grBb** from 195 to 140 nm (72%).

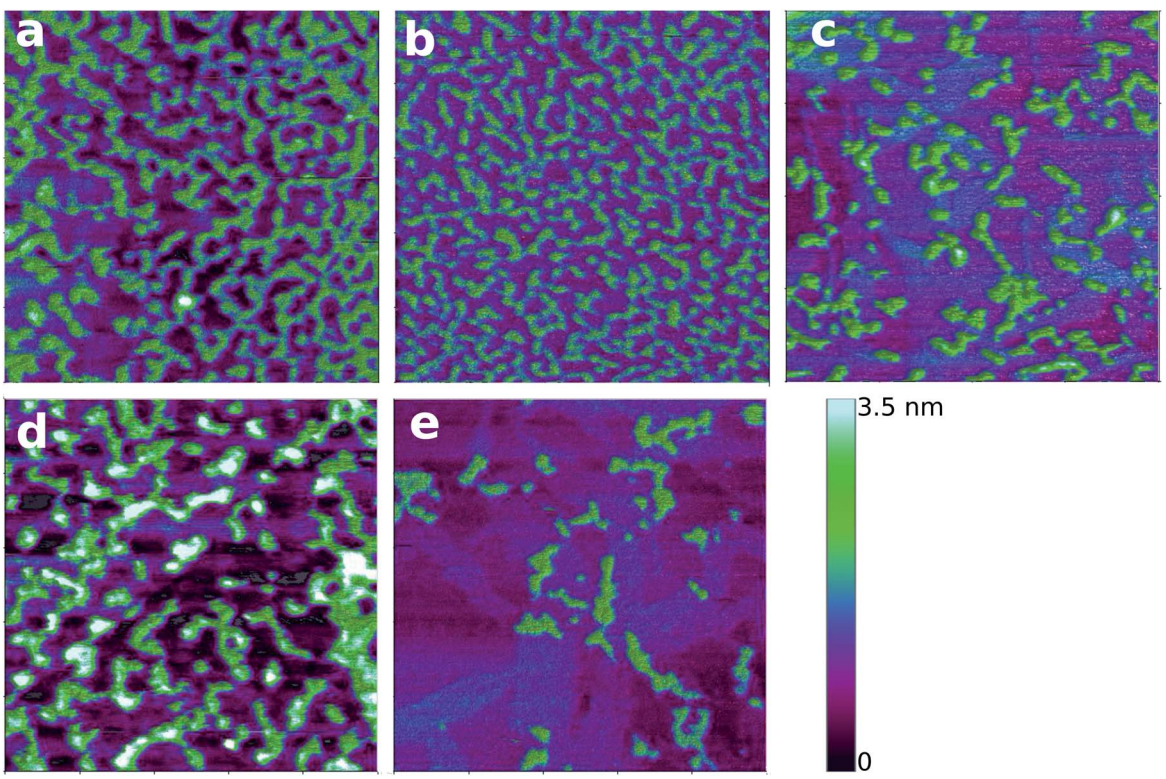

Fig. 2 AFM height image of bottlebrushes deposited on the HOPG surface in air (a) **Bb1**, (b) **Bb2**, (c) **Bb3**, (d) **Bb4** and (e) **grBb** (scan sizes: 500 nm × 500 nm. *z*-scales: 3.5 nm).

The LCST temperature was found to be around 32 °C in all cases, but different types of LCST behavior were observed. Previously, Matyjaszewski and coworkers[67] showed for temperature responsive bottlebrush molecules that due to the compact structure of molecular brushes, intramolecular collapse can occur when the average distance between molecules is much larger than the hydrodynamic dimensions of the individual macromolecules. However, if the concentration of the solution of molecular brushes is increased to the level in which the separation distance is comparable with the brush hydrodynamic dimensions, intermolecular aggregation occurs, as typically observed for solutions of linear polymers.[68] In another study on poly(thiophene)-*g*-**PNIPAM**,[15] a twofold decrease in size was found accompanied by a coil-to-collapsed globule transition, but no intermolecular aggregation occurred. **Bb2** showed intermolecular collapse above the LCST, at similar solution concentrations to the above examples. This behavior is likely caused by the longer **PNIPAM** chains present in **Bb2** compared to **Bb3** and **grBb**, and by the uncleaved *n*-dodecyl end groups originating from the RAFT initiator that were removed in the case of **Bb3** and **grBb**. The relatively large R_h measured for **grBb** suggests

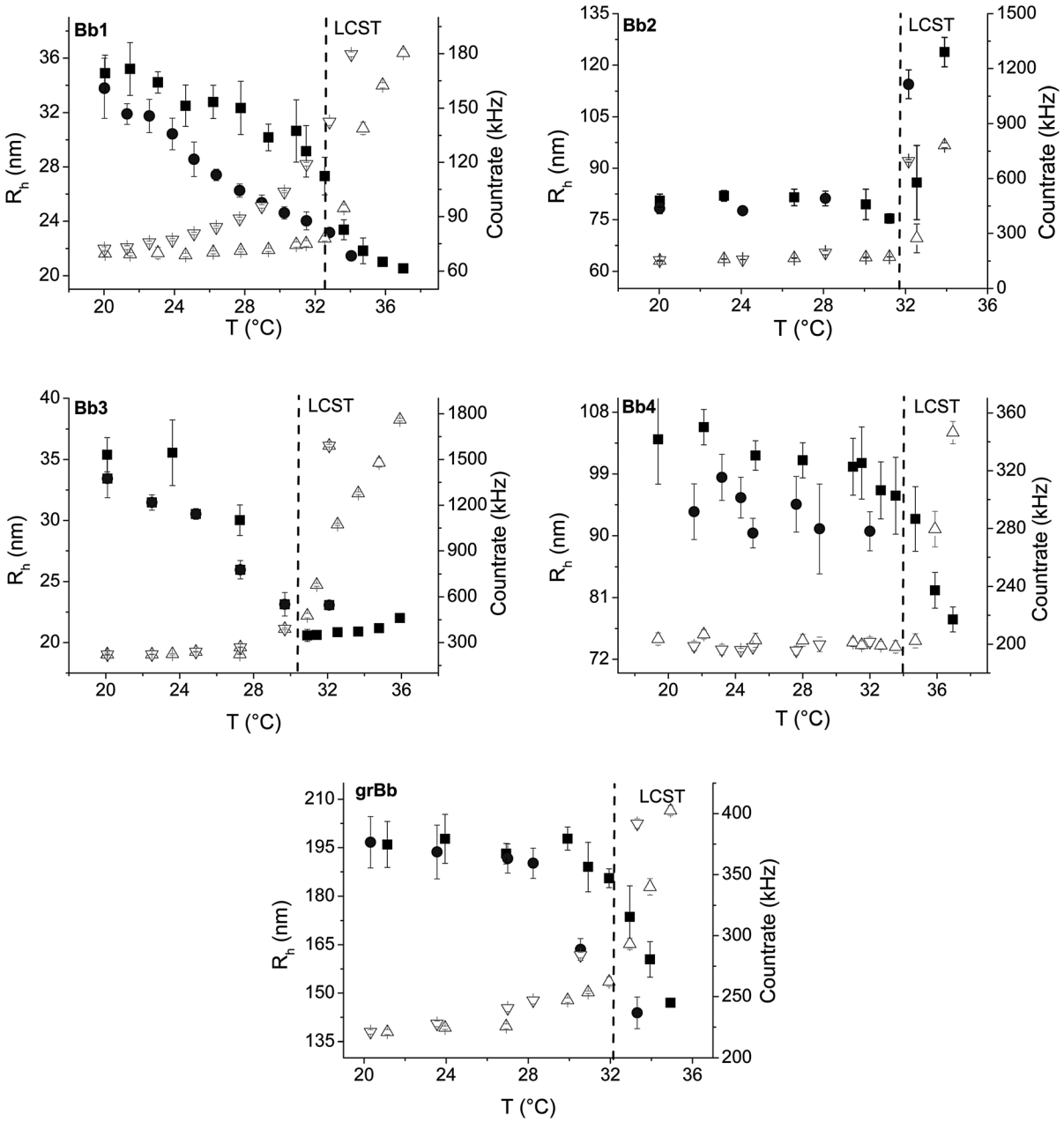

Fig. 3 Dependence of the hydrodynamic radius R_h (nm) (squares: heating, circle: cooling) and the scattering light intensities countrate (kHz) (up-triangle: heating, down-triangle: cooling) on the temperature of **Bb1**, **Bb2**, **Bb3**, **Bb4** and **grBb** measured by DLS. Upon heating **Bb1**, **Bb3**, **Bb4** and **grBb** collapse at T_{LCST} while **Bb2** shows aggregation. All bottlebrushes regained their size upon cooling back to 20 °C. The countrate increases sharply at the T_{LCST}, and decreases while the molecules rehydrate.

that these bottlebrushes, possessing a hydrophobic tail, formed micellar aggregates in aqueous solution.

The dimension range of the bottlebrushes obtained by DLS matched well with that obtained by AFM, however the size depends on the hydration of the molecules. The size of the macromolecules decreased gradually with temperature until the LCST.[4,19,69,70] The original size of the molecules was recovered after cooling, showing a hysteresis due to delayed dehydration and hydration of the densely grafted **PNIPAM** chains. Static light scattering measurements are summarized in the ESI.†

2.5 Electrochemical response of the bottlebrushes

The electrochemical behavior of the bottlebrushes on freshly cleaved, atomically smooth HOPG surfaces was investigated by cyclic voltammetry (CV) and differential pulse voltammetry (DPV). Due to the presence of Fe in the repeat units of the polymer chain and due to intermetallic coupling, PFS shows a distinctive electrochemical response.[26,27]

Cyclic voltammograms typically display two reversible oxidation and reduction peaks, associated with the stepwise, one-electron oxidation of the Fe atoms in the PFS backbone. CVs of **Bb1**, **Bb3**, **Bb4** and **grBb** were recorded between 0 and 0.8 V with HOPG as a working electrode, Ag/AgCl as the reference electrode and Pt as a counter electrode in 0.1 M $NaClO_4$ electrolyte solution, at 22 and 35 °C (Fig. S15, ESI†). Fig. 4 shows a typical example of the recorded electrochemical behavior of the physisorbed bottlebrushes. The CVs of the bottlebrushes show the double oxidation and reduction waves. At elevated scan rates, the two oxidation and reduction waves were less well-resolved, likely due to slow electron transfer.[71]

Below the LCST, the peak current showed a linear dependence on the scanning rate, indicating typical surface-confined electron transport, *i.e.* the presence of adsorbed molecules on the electrode (HOPG) surface. However, above the LCST, in some cases, neither the scan rate (ν) nor its square root ($\nu^{1/2}$) scaled linearly to the peak current, as would be the case for pure diffusion-controlled electron transport, suggesting an insulating effect of the collapsed side chains (Fig. 4). The peak potentials of the recorded CVs are presented in Table 5.

The electrochemical behavior of the molecular brushes was investigated further by differential pulse voltammetry (DPV). DPV curves were acquired at 5 mV s^{-1} scan rate, 50 ms pulse time, 200 ms interval time, 10 mV pulse height between 0 and 0.8 V, using HOPG as a working electrode, Ag/AgCl as the reference electrode and Pt as a counter electrode in 0.1 M $NaClO_4$ electrolyte solution. DPV curves of bottlebrushes **Bb1**, **Bb3**, **Bb4** and **grBb** (Fig. 5, S16 and S17, ESI†) show two reversible redox signals typical of PFSs, indicating intermetallic coupling between neighboring iron centers in the polymer chain. DPV curves were obtained both at room temperature and

Table 5 Oxidation and reduction peak positions of the bottlebrushes deposited on the HOPG surface measured in 0.1 M aqueous $NaClO_4$

	E_{ox1}	E_{ox2} (V)	E_{red2}	E_{red1}
Bb1	0.41	0.57	0.54	0.36
Bb2	0.5			
Bb3	0.40	0.57	0.54	0.34
Bb4	0.39	0.54	0.51	0.34
grBb	0.44	0.57	0.54	0.40

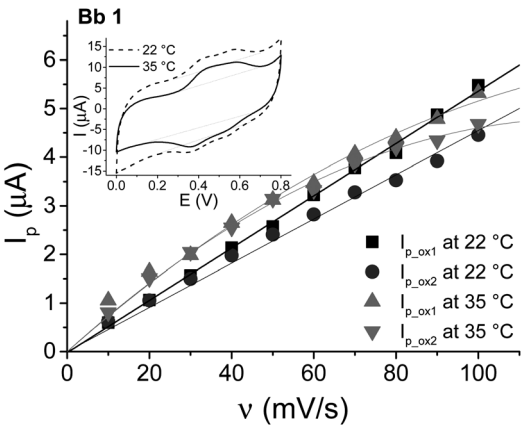

Fig. 4 Dependence of peak currents *versus* scan rates of **Bb1** adsorbed on the HOPG electrode. Reference electrode Ag/AgCl, counter electrode Pt, 0.1 M aqueous $NaClO_4$. Insets show the cyclic voltammograms recorded at a scan rate of 50 mV s^{-1}.

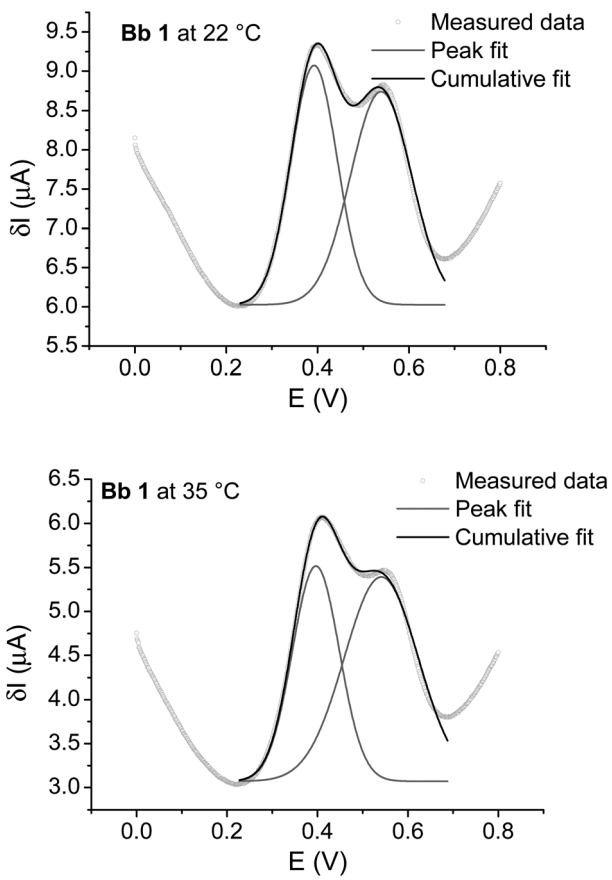

Fig. 5 Differential pulse voltammograms recorded of **Bb1**: (a) at 22 °C, (b) 35 °C adsorbed on HOPG (ν = 5 mV s^{-1} scan rate, 50 ms pulse time, 200 ms interval time, 10 mV pulse height reference electrode Ag/AgCl, counter electrode Pt, 0.1 M aqueous $NaClO_4$).

above the LCST to determine whether the temperature influences the relative amounts of ferrocene units involved in the electron transfer steps. The DPV curves were fitted by Gaussian approximation. In each case, the best fit was obtained by employing two peaks to describe the measured curve.

As earlier mentioned, ferrocene units along the PFS chain in alternating positions oxidize in the first oxidation wave, followed by oxidation of the remaining ferrocenes in the second wave at higher potential. Therefore, the ratio of the two peaks should be 1 : 1.[26,27] If interchain contributions (and higher neighbor contributions for the same chain, *i.e.*, by looping) are also present, the ratio between the first and the second wave of the corresponding oxidation steps may vary and differ from 1 : 1[26,27] relative weights. Bulk electrochemistry performed on PFS homopolymers in dilute solutions (5 mM PFS in CH_2Cl_2 with 0.1 M Bu_4NPF_6 as the supporting electrolyte) showed that ferrocene sites are oxidized stepwise with a relative ratio of 1 : 1 between the two oxidation peaks. Under these conditions, no interchain interactions and only intramolecular Fe–Fe interactions occur. Thus, in dilute solution, each ferrocene has two immediate neighbors. Due to the presence of the **PNIPAM** side chains, intra- and interchain interactions for the PFS backbone in the bottlebrushes are unlikely to occur and for all bottlebrushes, independent of the temperature, 1 : 1 relative weights were observed for the first and second oxidation waves.

In contrast to the above mentioned bottlebrushes, a "break-in" behavior[72] was observed in the case of **Bb2** upon oxidation at 22 °C (Fig. 6). No double oxidation and reduction waves are visible in the CV of **Bb2** and oxidation occurred at a higher potential ($E_{ox} = 0.5$ V) than that found for the first wave of the other bottlebrushes. When the PFS backbone is surrounded by a larger amount of redox inactive (insulating) polymer, the chain becomes less accessible for electron transfer. If the backbone is adsorbed *via* the side chains onto the electrode surface and side chains prevent the backbone and the electrode to be in close proximity, electron transfer becomes slow due to limitations caused by the **PNIPAM** layer. This was confirmed by the fact that upon increasing the scan rate, the PFS backbone remained unoxidized, and in response to oxidation **Bb2** desorbed from the electrode surface, as was evident from the intensity of the peak current which decreased after multiple cycles. As the temperature was increased to above the **PNIPAM** LCST, **Bb2** precipitated. At 34 °C, the **PNIPAM** chains around the PFS backbone collapsed, thereby forming a more dense layer between the electrode surface and the backbone, now acting as an insulator.[73] As a result, electron transfer to the PFS backbone became more difficult and a CV could not be measured. The bottlebrush structure therefore directly influences the redox behavior of the macromolecule. In addition to the **PNIPAM** chain length and grafting density, the end group of the bottlebrush grafts may also influence charge transport between the electrode and the PFS backbone. For example, in contrast to **Bb3** and **grBb**, **Bb2** still possessed *n*-dodecyl end groups at its **PNIPAM** chain ends that may further inhibit charge transport.

As both the backbone and the side chains can be directly, independently addressed, sequentially applied stimuli may introduce translocation of the surface confined molecules. The gradient bottlebrushes possess an asymmetrical architecture along their backbone, which can be a key to induce stimuli

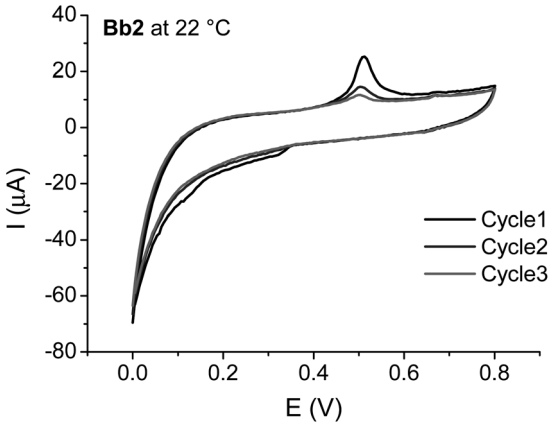

Fig. 6 Cyclic voltammogram of **Bb2** at 22 °C adsorbed on the HOPG electrode. The cyclic voltammogram shows 'break-in' behavior and the polymer layer depletes from the surface after multiple cycles. Reference electrode Ag/AgCl, counter electrode Pt, 0.1 M aqueous $NaClO_4$.

triggered directed molecular motion by switching between the hydrophilic/hydrophobic surface of **PNIPAM** and the redox-induced lengthening/shortening of the PFS backbone.[74] Such surface confined "nanocrawlers" are candidates to carry and deliver molecular payloads in future nanoscale devices.

3 Summary and conclusion

Water soluble dual stimuli responsive PFS-*g*-**PNIPAM** molecular bottlebrushes were obtained using "grafting to" and "grafting from" processes. After quantitative azide functionalization of the PFS main chain, **PNIPAM** chains were attached to the backbone *via* a click reaction. Approximately 75% of the azide groups were engaged, yielding worm like bottlebrushes with relatively high grafting density. Being deposited on a HOPG surface, the bottlebrushes displayed the typical electrochemical behavior of single PFS chains lacking intra- and intermolecular interactions. CV and DPV results show that the bottlebrush architecture strongly influences its redox behavior. In most cases the ferrocene units are in close proximity to the HOPG electrode surface and are accessible to the supporting electrolyte ions because of the hydrophilic **PNIPAM** side chains. However, when hydrophobic *n*-dodecyl end groups were present at the **PNIPAM** side chain ends, charge transport between the electrode and the PFS backbone was found to be inhibited. A composition gradient of clickable and inert ferrocenylsilane repeat units in the PFS backbone was successfully achieved, resulting in an asymmetrical bottlebrush molecule. In an aqueous solution, the gradient bottlebrush molecules self-assembled into micelles through hydrophobic interactions of their tails.

4 Experimental section

Materials

Chemicals were purchased from Sigma-Aldrich (the Netherlands) and were used as received if not stated otherwise. Organic solvents were purchased from Biosolve (Valkenswaard,

the Netherlands). *N*-isopropylacrylamide (Acros Organics, Belgium) was recrystallized from hexane/toluene. Deuterated chloroform was purchased from Buchem BV (Apeldoorn, the Netherlands). CuCl and CuBr were added in 98% acetic acid, stirred overnight, filtered, washed with methanol and dried under vacuum. Deionized water from a MilliQ Advantage A 10 purification system (Millipore, Billerica, Ma, USA) was used. For dialysis, Spectra/Por membranes with $M_w = 1000$ or 15 000 g mol^{-1} cut off were used. Tris((dimethylamino)ethyl)amine (Me_6TREN) was purchased from Alfa Aesar (USA). Basic aluminum oxide 60 was purchased from Merck KGaA (Darmstadt, Germany). Ascorbic acid was received from Fluka.

Methods

NMR spectroscopy. ^{1}H NMR spectra were recorded on a Varian Unity Inova (300 MHz) or on a Bruker Avance (400 MHz) instrument. ^{13}C NMR was carried out at 75.5 MHz, on a Varian Unity Inova (300 MHz) instrument. As a reference, the chemical shift of the solvent signal ($CDCl_3$) $\delta = 7.26$ ppm was used.

FTIR spectroscopy. Single reflection attenuated total reflection (ATR) mode FTIR spectra (spectral resolution 4 cm^{-1}, 32 scans) were recorded with a Bruker model Alpha FTIR spectrometer equipped with an ATR platinum diamond 1 reflection crystal (Bruker Optik GmbH, Ettlingen, Germany). Before measurements a background spectrum was recorded against air.

Dynamic Light Scattering. DLS measurements were performed on an ALV instrument equipped with an ALV7002 external correlator and a 300 mW Cobolt Samba-300 DPSS laser operating at a wavelength of 532 nm. The data were recorded at 90° scattering angle. The samples were contained in glass cells and thermostatted at the required temperature.

Electrochemical measurements. Electrochemical measurements were carried out on an AutoLab PGSTAT 10 electrochemical workstation. Typically, 1–2 mg bottlebrush containing 0.1 M $NaClO_4$ aqueous solution was used for the measurements, in which the electrodes were immersed. HOPG was used as a working electrode, and Pt wire was used as a counter electrode against an Ag/AgCl reference electrode. Voltammograms were recorded at different scan rates 10, 20, 50 and 100 mV s^{-1} and between 0 and 0.8 V. Differential pulse voltammograms were measured with $\nu = 5$ mV s^{-1} scan rate, 50 ms pulse time, 200 ms interval time, and 10 mV pulse height. The baseline (assumed to be linear) was determined manually for all measurements and subtracted from the measurement data.

Atomic force microscopy. A Bruker Multimode AFM and a NanoScope V controller were used and operated in PeakForce tapping mode in air (Bruker/Veeco, Santa Barbara, CA).

Gel Permeation Chromatography (GPC). GPC measurements on the polymers were carried out in THF (flow rate 2.0 mL min^{-1}) at 25 °C, using microstyragel columns (bead size 10 μm) with pore sizes of 10^5, 10^4, 10^3, and 500 Å (Waters) and in 0.1 LiCl/DMF (flow rate 1.0 mL min^{-1}) at 25 °C, using microstyragel columns (bead size 10 μm) with pore sizes of 10^5, 10^4, 10^3, and 10^6 Å (Waters), with a differential refractometer (Waters model 410) detection system. Molar masses were determined relative to polystyrene standards in THF and relative to poly(methyl methacrylate) standards in DMF.

Synthesis of 1a

In a glovebox under prepurified N_2, [**1**](3-chloropropyl)-methylsilaferrocenophane, (0.86 g, 2.8 mmol) was dissolved in THF (13 mL), and the polymerization was started by adding the catalyst, $H_2PtCl_6 \cdot 6H_2O$ (15 mg, 3×10^{-5} mol). The solution was continuously stirred and after 1, 2 and 3 hours additional monomers were introduced, [**1**]ethylmethylsilaferrocenophane (0.82 g, 3.2 mmol) dissolved in THF (13 mL), [**1**]ethylmethylsilaferrocenophane (0.51 g, 2.0 mmol) dissolved in THF (10 mL) and (3-chloropropyl)methylsilaferrocenophane (0.27 g, 0.9 mmol) dissolved in THF (10 mL), respectively. The polymerization was conducted for 8 h in total and precipitation in MeOH afforded **1a** (0.60 g, 50%) as an orange-yellow solid. $T_g = 10$ °C. ^{1}H NMR (300 MHz, $CDCl_3$, ppm): 0.4 (s, 3H, $CH_3SiCH_2CH_3$), 0.5 (s, 3H, CH_3Si), 0.9 (m, 2H, $SiCH_2CH_3$), 1.0 and 1.1 (m, $SiCH_2CH_2CH_2$ and $SiCH_2CH_3$), 1.8 (m, 2H, $SiCH_2$–CH_2CH_2), 3.5 (m, 2H, $SiCH_2CH_2CH_2Cl$), 4.0 and 4.2 (m, 4-4H, *Cp*); ^{13}C NMR (100 MHz, $CDCl_3$, ppm): −3.3 ($CH_3SiCH_2CH_3$), –3.05 (CH_3Si), 8.15 ($SiCH_2CH_3$), 14.1 ($SiCH_2CH_2$–), 28.0 ($SiCH_2CH_2$–), 48.4 (–CH_2CH_2N), 70.2 (*Cp*Si–), 70.7 (*Cp*$SiCH_2CH_3$), 71.4 and 73.6 (*Cp*); ATR-FTIR (wavenumbers (cm^{-1})): 3086, 2931, 2870, 1447, 1420, 1380, 1360, 1160, 1034, 892, 865, 826, 771, 742.

Synthesis of 3

Either **1** or **2** was used as a starting material to obtain poly(ferrocenyl(3-azidopropyl)methylsilane) **3**. **2** (530 mg, 1.34 mmol), NaN_3 (260 mg, 4 mmol) and 15-crown-5 (800 mg, 3.6 mmol, 0.7 mL) were dissolved in THF (12 mL) and stirred for 16 days in a N_2 atmosphere. The polymer was precipitated twice in MeOH. **1** (300 mg, 1 mmol), NaN_3 (320 mg, 5 mmol) and 15-crown-5 (460 mg, 2.06 mmol, 0.4 mL) were dissolved in the mixture of THF (10 mL) and DMSO (2 mL), heated to 50 °C and stirred for 16 days in a N_2 atmosphere, yielding **3**. The product was precipitated twice in MeOH and dried in a vacuum. ^{1}H NMR (300 MHz, $CDCl_3$): 0.45 (s, 3H, (CH_3Si), 0.9 (m, 2H, $SiCH_2CH_2CH_2$), 1.7 (m, 2H, $SiCH_2CH_2CH_2$), 3.25 (m, 2H, $SiCH_2CH_2CH_2$–), 3.9 and 4.15 (m, 4-4H, *Cp*); ^{13}C NMR (75 MHz, $CDCl_3$): −3.4 (CH_3Si), 13.4 ($SiCH_2CH_2$–), 23.9 ($SiCH_2CH_2$–), 54.2 (–CH_2CH_2N), 69.8 (Si*Cp*), 71.3 and 73.2 (*Cp*); ATR-FTIR (wavenumbers (cm^{-1})): 3086, 2931, 2870, 2088, 1447, 1420, 1380, 1360, 1247, 1160, 1034, 892, 865, 826, 771, 742.

Synthesis of 3a

1a (300 mg, 1 mmol), NaN_3 (320 mg, 5 mmol) and 15-crown-5 (460 mg, 2.06 mmol, 0.4 mL) were dissolved in a mixture of THF (10 mL) and DMSO (2 mL), heated to 50 °C and stirred for 2.5 weeks in a N_2 atmosphere. The product was precipitated twice in MeOH and dried in a vacuum. ^{1}H NMR (300 MHz, $CDCl_3$, ppm): 0.4 (s, 3H, $CH_3SiCH_2CH_3$), 0.5 (s, 3H, CH_3Si), 0.9 (m, 2H, $SiCH_2CH_3$), 1.0 and 1.1 (m, $SiCH_2CH_2CH_2$ and $SiCH_2CH_3$) 1.6 (m, 2H, $SiCH_2CH_2CH_2$), 3.2 (m, 2H, $SiCH_2CH_2CH_2$ Cl), 4.0 and 4.2 (m, 4-4H, *Cp*); ATR-FTIR (wavenumbers (cm^{-1})): 3086, 2931, 2870, 2088, 1447, 1420, 1380, 1360, 1247, 1160, 1034, 892, 865, 826, 771, 742.

Synthesis of ATRP initiator

3-(Trimethylsilyl)prop-2-yn-1-yl-2-chloropropanoate was synthesized according to the literature.[59] The product, a yellowish oil, was purified by flash chromatography (*n*-heptane/EtOAc) 19 : 1. ^{1}H NMR (300 MHz, $CDCl_3$): 0.2 (s, 9H, $CH_3)_3$Si), 1.7 (d, 3H, CH(Cl)CH_3), 4.4 (q, 1H, H(Cl)CH_3), 4.7 (m, 2H, –CHCH_2O–); ^{13}C NMR (75 MHz, $CDCl_3$): −0.3 (CH_3Si), 21.3 (CH(Cl)CH_3), 52.0 (–CHCH_2O–), 54.1 (CH(Cl)CH_3), 93.0 and 97.9 (Si $C{\equiv}C$$CH_2$), 169.3 (–$C$(O)O–).

Synthesis of PNIPAM$_{13k}$ by ATRP

The initiator (3-(trimethylsilyl)prop-2-yn-1-yl-2-chloropropanoate) (232 mg, 1.1 mmol) was charged in an ampoule and evacuated while freezing with liquid N_2. At room temperature, the flask was backfilled with Ar, CuCl (106 mg, 1 mmol) was added and the system was frozen and evacuated again. Me_6 TREN (258 mg, 1.1 mmol, 300 μL) was dissolved in i-PrOH–DMF (1 mL) purged with Ar and added to the reaction flask. After complete dissolution of the CuCl, the monomer (6 g, 0.05 mol) dissolved in i-PrOH–DMF (8 mL) was added and the reaction mixture was degassed in three freeze–pump–thaw cycles and backfilled with Ar. After stirring for 16 h at room temperature, the reaction was terminated by exposure to air. The solvent was evaporated and the polymer was redissolved in chloroform and passed through a basic Al_2O_3 column to remove copper. The eluent was concentrated and the polymer was precipitated in Et_2O and dried in a vacuum. The polymer and Bu_4NF (156 mg) were stirred overnight in THF (50 mL) to remove the protecting group. The **PNIPAM** was precipitated from $CHCl_3$ to Et_2O, redissolved in water and dialysed (tubing: cut off Mw 1000 g mol^{-1}) until its solution became transparent. Yield 2.0 g. ^{1}H NMR (300 MHz, $CDCl_3$): 0.2 (s, 9H, $CH_3)_3$Si), 1.1 (s, 6H, –CH$CH_3)_2$), 1.5–2.0 (br m, 3H, –$CHCH_2$–), 4.0 (s, 1H, –$CH$$CH_3)_2$.

Synthesis of PNIPAM$_{7k/30k}$ by RAFT

PNIPAM$_{7k}$ and **PNIPAM**$_{30k}$ were synthesized according to a literature procedure.[58] ^{1}H NMR (300 MHz, $CDCl_3$): 0.9 (s, 3H, –$CH_2)_{10}CH_3$), 1.1 (s, 6H, –CH$CH_3)_2$), 1.25 (s, 20H, –$CH_2)_{10}CH_3$), 1.5–2.0 (br m, 3H, –$CHCH_2$–), 4.0 (s, 1H, –$CH$$CH_3)_2$, 4.7 (s, 2H, –$CH_2$O–); ATR-FTIR (wavenumbers (cm^{-1})): 3289, 3078, 2971, 2933, 2874, 1635, 1535, 1458, 1386, 1366, 1170.

Synthesis of Bb1

3$_{373k}$ (50 mg, 0.16 mmol), **PNIPAM**$_{13k}$ (1 g), CuBr (32 mg, 0.24 mmol), PMDETA (25 mg, 0.14 mmol), and ascorbic acid (traces) were dissolved in THF (10 mL) in a N_2 atmosphere. The mixture was stirred for 6 weeks. The solvent was removed, and the bottlebrush was dissolved in water and dialysed for 2 weeks using a membrane with 15 kDa cut off to remove the unreacted side chains. The polymer was stored in water at 4 °C.

Synthesis of Bb2 and Bb3

3$_{284k/376k}$ (50 mg, 0.16 mmol), **PNIPAM**$_{7k/30k}$ (1.8/1 g), $CuSO_4$ (32 mg, 0.24 mmol), PMDETA (25 mg, 0.14 mmol) and sodium ascorbate (80 mg) were dissolved in a mixture of THF (20 mL) and DMSO (1–2 mL) in a N_2 atmosphere. The mixture was stirred for two weeks. The solvent was removed, and the bottlebrush was dissolved in water and dialysed for two weeks using a membrane with 50 kDa cut off to remove the unreacted side chains. For end group deprotection, **Bb3** (170 mg) was dissolved in DMF (40 mL), and sodium dithionite was added. The solution was purged with Ar for 1 h and subsequently 1-hexylamine (100 μL) was added. The solution was stirred overnight, concentrated by removing the solvent under reduced pressure and the polymer was precipitated in Et_2O. The product and NIPAM (63 mg, 0.56 mmol) were dissolved in THF (10 mL) and 1-hexylamine (100 μL) was added. After stirring for 2 h, the product was precipitated twice in Et_2O and dried under N_2 stream. The polymer was stored in water at 4 °C. ^{1}H NMR (300 MHz, $CDCl_3$): 0.47 (s, CH_3Si), 0.9 (m, Si$CH_2CH_2CH_2$), 1.15 (br s, –NCH($CH_3)_2$), 1.6 (m, Si$CH_2CH_2CH_2$), 1.9–2.2 (br m, –$CHCH_2$–), 3.2 (s, Si$CH_2CH_2CH_2$–), 4.0 (br m, –N$CH$$(CH_3)_2$ and Cp), 4.2 (m, Cp); ATR-FTIR (wavenumbers (cm^{-1})): 3289, 3078, 2971, 2933, 2874, 1635, 1535, 1458, 1386, 1366, 1170, 1037.

Synthesis of grBb

3a (98 mg, 0.32 mmol) and **PNIPAM**$_{30k}$ (600 mg, mmol) were dissolved in a mixture of THF (5 mL) and DMSO (1 mL). $CuSO_4$ (30 mg, 0.20 mmol) and sodium ascorbate (80 mg, 0.4 mmol) were introduced in a N_2 atmosphere, and then PMDETA (57 μL, 0.4 mmol) was added. The reaction mixture was stirred for 5 days. Azide functionalized Merrifield resin[75] was added to remove the unreacted **PNIPAM** chains. The resin and the copper were removed by centrifugation, and the product was further purified by dialysis in MeOH and precipitation in Et_2O. **grBb** (150 mg) was dissolved in DMF (40 mL), sodium dithionite was added and after purging with Ar for 1 h 1-hexylamine (30 μL) was added. The solution was stirred overnight, concentrated by removing the solvent under reduced pressure and the polymer was precipitated in Et_2O. The product and NIPAM (110 mg, 1 mmol) were dissolved in THF (10 mL) and 1-hexylamine (100 μL) was added. After stirring for 2 h, the product was precipitated twice in Et_2O and dried under N_2 stream. ^{1}H NMR (400 MHz, $CDCl_3$, ppm): 0.46 (s, CH_3SiCH_2CH_3 and CH_3Si), 0.9 (m, SiCH_2CH_3), 1.1 (m, Si$CH_2CH_2CH_2$ and SiCH_2CH_2), 1.6 and 1.8 (bs, –CH_2CH–(**PNIPAM**) and Si$CH_2CH_2CH_2$), 2.1 (b m, –CH_2CH–(**PNIPAM**)), 3.5 (m, Si$CH_2CH_2CH_2$Cl), 4.0 and 4.2 (m, –HC$(CH_3)_2$ and 4-4H, Cp); ^{13}C NMR (100 MHz, $CDCl_3$, ppm): −3.3 (CH_3Si and CH_3SiCH_2CH_3), 7.94 and 7.88 (SiCH_2CH_3), 14.05 (SiCH_2CH_2–), 22.5 (–C$(CH_3)_2$), 35.8 (–NH$CH$$(CH_3)_2$), 41.26 and 42.6 (–CH$CH_2$– and $CH$$CH_2$–), 70.5 ($Cp$Si–), 70.7 ($CpSiCH_2CH_3$), 71.15 and 73.36 ($Cp$), 174.3 (–$C$(=O)NH–); ATR-FTIR (wavenumbers (cm^{-1})) 3289, 3078, 2971, 2933, 2874, 1635, 1535, 1458, 1386, 1366, 1170, 1037.

Synthesis of 5

4 was synthesized according to the literature.[33,63] Solution of **4** (0.49 mmol repeat units) in dichloromethane was cooled to −70 °C and Et_3N (0.15 g, 1.4 mmol) was added. Subsequently a solution of 2-chloropropionyl chloride (0.126 mg, 1 mmol) in CH_2Cl_2 (10 mL) was added dropwise. The solution was stirred

for 2 days, approaching room temperature. **5** was precipitated twice in MeOH. ^{1}H NMR (300 MHz, $CDCl_3$): 0.45 (s, 3H, CH_3Si), 0.9 (m, 2H, Si$CH_2$$CH_2CH_2$), 1.6 (m, 2H, $SiCH_2CH_2CH_2$), 1.7 (m, 3H, CH(Cl)CH_3), 3.2 (m, 2H, $SiCH_2CH_2CH_2$–), 4.0 and 4.2 (m, 4-4H, *Cp*), 4.4 (q, 1H, *CH*(Cl)CH_3); ^{13}C NMR (75 MHz, $CDCl_3$) of **5**–3.4 (CH_3Si), 13.3 (SiCH_2CH_2–), 22.8 (–CHCH_3), 24.1 ($SiCH_2CH_2$–), 42.7 (–CH_2CH_2N), 56.0 (CCH_2Cl), 65.5 (–Si*Cp*), 71.3 and 73.2 (*Cp*), 169.4 (–*C*(=O)N–); ATR-FTIR (wavenumbers (cm^{-1}) 3290, 3083, 2949, 2870, 1655, 1528, 1441, 1420, 1379, 1362, 1247, 1161, 1035, 909, 892, 865, 828, 772.

Synthesis of Bb4

5 (80 mg, 0.37 mmol repeat units) was dissolved in THF (5 mL) and purged with Ar to remove oxygen from the solution. $CuBr_2$ (30 mg, 0.2 mmol) and a solution of NIPAM (1.0 g, 8.8 mmol) and Me_6TREN (80 μL, 0.4 mmol) in THF (5 mL) and DMF (1 mL) were added, and the mixture was purged further. The polymerization was started by adding ascorbic acid (100 mg). After 48 h, the polymerization was terminated by opening the reaction vial to air. The polymer was precipitated in Et_2O, redissolved in $CHCl_3$ and pressed through a basic Al_2O_3 column to remove the copper. The bottlebrush was then dissolved in water and dialyzed to remove all traces of the monomer and copper. The polymer was stored as an aqueous solution. ^{1}H NMR (400 MHz, $CDCl_3$): 0.47 (s, CH_3Si), 0.9 (m, Si$CH_2CH_2CH_2$), 1.15 (br s, –NCH(CH_3)$_2$), 1.6 (m, $SiCH_2CH_2CH_2$), 1.9–2.2 (bs, –$CHCH_2$–), 3.2 (m, $SiCH_2CH_2CH_2$–), 4.0 (br m, –NCH(CH_3)$_2$ and *Cp*), 4.2 (m, *Cp*); ATR-FTIR (wavenumbers (cm^{-1})): 3291, 3078, 2967, 2926, 2872, 1638, 1532, 1456, 1385, 1365, 1171, 1036.

Acknowledgements

The authors thank Dr Martien Cohen-Stuart (Wageningen University, the Netherlands) for the use of the light scattering instrument. Mr Remco Fokkink (Wageningen University, the Netherlands) is acknowledged for his help with light scattering measurements. We thank Mr Clemens Padberg (MESA$^+$ Institute, University of Twente, the Netherlands) for the GPC measurements. This work was financially supported by the MESA$^+$ Institute for Nanotechnology of the University of Twente and by the Netherlands Organization for Scientific Research (NWO, TOP Grant 700.56.322, Macromolecular Nanotechnology with Stimulus Responsive Polymers).

References

1 H.-i. Lee, J. R. Boyce, A. Nese, S. S. Sheiko and K. Matyjaszewski, *Polymer*, 2008, **49**, 5490–5496.
2 H. Liu, Y. Zhang, J. Hu, C. Li and S. Liu, *Macromol. Chem. Phys.*, 2009, **210**, 2125–2137.
3 H. Tang, Y. Li, S. H. Lahasky, S. S. Sheiko and D. Zhang, *Macromolecules*, 2011, **44**, 1491–1499.
4 C. M. Li, N. Gunari, K. Fischer, A. Janshoff and M. Schmidt, *Angew. Chem., Int. Ed.*, 2004, **43**, 1101–1104.
5 Y. Xu, S. Bolisetty, M. Drechsler, B. Fang, J. Yuan, L. Harnau, M. Ballauff and A. H. E. Müller, *Soft Matter*, 2009, **5**, 379.
6 M. A. Cohen-Stuart, W. T. S. Huck, J. Genzer, M. Müller, C. Ober, M. Stamm, G. B. Sukhorukov, I. Szleifer, V. V. Tsukruk, M. Urban, F. Winnik, S. Zauscher, I. Luzinov and S. Minko, *Nat. Mater.*, 2010, **9**, 101–113.
7 W. Yuan, J. Zhang, H. Zou, T. Shen and J. Ren, *Polymer*, 2012, **53**, 956–966.
8 J. A. Johnson, Y. Y. Lu, A. O. Burts, Y. Xia, A. C. Durrell, D. A. Tirrell and R. H. Grubbs, *Macromolecules*, 2010, **43**, 10326–10335.
9 A. Nese, N. V. Lebedeva, G. Sherwood, S. Averick, Y. Li, H. Gao, L. Peteanu, S. S. Sheiko and K. Matyjaszewski, *Macromolecules*, 2011, **44**, 5905–5910.
10 M. F. Zhang and A. H. E. Müller, *J. Polym. Sci., Part A: Polym. Chem.*, 2005, **43**, 3461–3481.
11 S. S. Sheiko, B. S. Sumerlin and K. Matyjaszewski, *Prog. Polym. Sci.*, 2008, **33**, 759–785.
12 H.-i. Lee, J. Pietrasik, S. S. Sheiko and K. Matyjaszewski, *Prog. Polym. Sci.*, 2010, **35**, 24–44.
13 F. A. Plamper, S. Reinicke, M. Elomaa, H. Schmalz and H. Tenhu, *Macromolecules*, 2010, **43**, 2190–2203.
14 C. Li, Z. Ge, J. Fang and S. Liu, *Macromolecules*, 2009, **42**, 2916–2924.
15 S. S. Balamurugan, G. B. Bantchev, Y. Yang and R. L. McCarley, *Angew. Chem., Int. Ed.*, 2005, **44**, 4872–4876.
16 M. Wang, S. Zou, G. Guerin, L. Shen, K. Deng, M. Jones, G. C. Walker, G. D. Scholes and M. A. Winnik, *Macromolecules*, 2008, **41**, 6993–7002.
17 G. L. Cheng, A. Boker, M. F. Zhang, G. Krausch and A. H. E. Müller, *Macromolecules*, 2001, **34**, 6883–6888.
18 J. Bolton and J. Rzayev, *ACS Macro Lett.*, 2012, **1**, 15–18.
19 D. Gromadzki, A. Jigounov, P. Stepanek and R. Makuska, *Eur. Polym. J.*, 2010, **46**, 804–813.
20 J. Yin, Z. Ge, H. Liu and S. Liu, *J. Polym. Sci., Part A: Polym. Chem.*, 2009, **47**, 2608–2619.
21 H. C. Kolb, M. G. Finn and K. B. Sharpless, *Angew. Chem., Int. Ed.*, 2001, **40**, 2004–2021.
22 N. Akeroyd and B. Klumperman, *Eur. Polym. J.*, 2011, **47**, 1207–1231.
23 Z. Zarafshani, O. Akdemir and J.-F. Lutz, *Macromol. Rapid Commun.*, 2008, **29**, 1161–1166.
24 W. H. Binder and R. Sachsenhofer, *Macromol. Rapid Commun.*, 2007, **28**, 15–54.
25 J. E. Moses and A. D. Moorhouse, *Chem. Soc. Rev.*, 2007, **36**, 1249–1262.
26 M. T. Nguyen, A. F. Diaz, V. V. Dement'ev and K. H. Pannell, *Chem. Mater.*, 1993, **5**, 1389–1394.
27 R. Rulkens, A. J. Lough, I. Manners, S. R. Lovelace, C. Grant and W. E. Geiger, *J. Am. Chem. Soc.*, 1996, **118**, 12683–12695.
28 D. A. Foucher, B.-Z. Tang and I. Manners, *J. Am. Chem. Soc.*, 1992, **114**, 6246–6248.
29 K. Temple, F. Jakle, J. B. Sheridan and I. Manners, *J. Am. Chem. Soc.*, 2001, **123**, 1355–1364.
30 D. A. Rider, K. A. Cavicchi, K. N. Power-Billard, T. P. Russell and I. Manners, *Macromolecules*, 2005, **38**, 6931–6938.
31 V. Bellas and M. Rehahn, *Angew. Chem., Int. Ed.*, 2007, **46**, 5082–5104.

32 M. Tanabe, G. W. M. Vandermeulen, W. Y. Chan, P. W. Cyr, L. Vanderark, D. A. Rider and I. Manners, *Nat. Mater.*, 2006, **5**, 467–470.
33 M. A. Hempenius, N. S. Robins, R. G. H. Lammertink and G. J. Vancso, *Macromol. Rapid Commun.*, 2001, **22**, 30–33.
34 J. F. Gohy, B. G. G. Lohmeijer, A. Alexeev, X.-S. Wang, I. Manners, M. A. Winnik and U. S. Schubert, *Chem.–Eur. J.*, 2004, **10**, 4315–4323.
35 Z. Wang, A. Lough and I. Manners, *Macromolecules*, 2002, **35**, 7669–7677.
36 X. Wang, M. A. Winnik and I. Manners, *Macromolecules*, 2005, **38**, 1928–1935.
37 M. A. Hempenius, F. F. Brito and G. J. Vancso, *Macromolecules*, 2003, **36**, 6683–6688.
38 K. N. Power-Billard and I. Manners, *Macromolecules*, 2000, **33**, 26–31.
39 X. Sui, M. A. Hempenius and G. J. Vancso, *J. Am. Chem. Soc.*, 2012, **134**, 4023–4025.
40 M. Y. Zaremski, D. I. Kalugin and V. B. Golubev, *Polym. Sci., Ser. A*, 2009, **51**, 103–122.
41 H.-i. Lee, K. Matyjaszewski, S. Yu and S. S. Sheiko, *Macromolecules*, 2005, **38**, 8264–8271.
42 S. J. Lord, S. S. Sheiko, I. LaRue, H.-I. Lee and K. Matyjaszewski, *Macromolecules*, 2004, **37**, 4235–4240.
43 W. A. Braunecker and K. Matyjaszewski, *Prog. Polym. Sci.*, 2007, **32**, 93–146.
44 U. Beginn, *Colloid Polym. Sci.*, 2008, **286**, 1465–1474.
45 D. Wu, X. Song, T. Tang and H. Zhao, *J. Polym. Sci., Part A: Polym. Chem.*, 2010, **48**, 443–453.
46 J. N. Kizhakkedathu, R. Norris-Jones and D. E. Brooks, *Macromolecules*, 2004, **37**, 734–743.
47 A. E. Smith, X. Xu and C. L. McCormick, *Chem. Commun.*, 2010, **35**, 45–93.
48 P.-E. Millard, N. C. Mougin, A. Böker and A. H. E. Müller, in *Controlling the Fast ATRP of N-Isopropylacrylamide in Water*, ed. K. Matyjaszewski, American Chemical Society, Washington DC, 2009, ch. 10, pp. 127–137.
49 J. Xu, J. Ye and S. Liu, *Macromolecules*, 2007, **40**, 9103–9110.
50 J. Ye and R. Narain, *J. Phys. Chem. B*, 2009, **113**, 676–681.
51 H. G. Schild, *Prog. Polym. Sci.*, 1992, **17**, 163–249.
52 Y. Zhang, S. Furyk, L. B. Sagle, Y. Cho, D. E. Bergbreiter and P. S. Cremer, *J. Phys. Chem. C*, 2007, **111**, 8916–8924.
53 O. Boissiere, D. Han, L. Tremblay and Y. Zhao, *Soft Matter*, 2011, **7**, 9410–9415.
54 J. D. Kretlow, M. C. Hacker, L. Klouda, B. B. Ma and A. G. Mikos, *Biomacromolecules*, 2010, **11**, 797–805.
55 Y.-J. Liu, A. Pallier, J. Sun, S. Rudiuk, D. Baigl, M. Piel, E. Marie and C. Tribet, *Soft Matter*, 2012, **8**, 8446–8455.
56 Y. Xia, N. A. D. Burke and H. D. H. Stöver, *Macromolecules*, 2006, **39**, 2275–2283.
57 M. Malkoch, K. Schleicher, E. Drockenmuller, C. J. Hawker, T. P. Russell, P. Wu and V. V. Fokin, *Macromolecules*, 2005, **38**, 3663–3678.
58 J. Chen, M. Liu, C. Chen, H. Gong and C. Gao, *ACS Appl. Mater. Interfaces*, 2011, **3**, 3215–3223.
59 J. A. Opsteen and J. C. M. van Hest, *Chem. Commun.*, 2005, 57–59.
60 J. W. Chan, C. E. Hoyle, A. B. Lowe and M. Bowman, *Macromolecules*, 2010, **43**, 6381–6388.
61 G. Socrates, *Infrared Characteristic Group Frequencies: Tables and Charts*, John Wiley & Sons Ltd., Chichester, 2nd edn, 1994.
62 X. Sui, X. Feng, A. Di Luca, C. A. van Blitterswijk, L. Moroni, M. A. Hempenius and G. J. Vancso, *Polym. Chem.*, 2013, **4**, 337.
63 C. F. C. Fitie, E. Mendes, M. A. Hempenius and R. P. Sijbesma, *Macromolecules*, 2011, **44**, 757–766.
64 K. Min, H. Gao and K. Matyjaszewski, *Macromolecules*, 2007, **40**, 1789–1791.
65 A. A. Steinschulte, B. Schulte, N. Drude, M. Erberich, C. Herbert, J. Okuda, M. Möller and F. A. Plamper, *Polym. Chem.*, 2013, **4**, 3885.
66 C. Wu and S. Zhou, *J. Macromol. Sci., Part B: Phys.*, 1997, **836**, 345–355.
67 J. Pietrasik, B. S. Sumerlin, R. Y. Lee and K. Matyjaszewski, *Macromol. Chem. Phys.*, 2007, **208**, 30–36.
68 K. Kubota, S. Fujishige and I. Ando, *J. Phys. Chem.*, 1990, **94**, 5154–5158.
69 J. Zhao, G. Mountrichas, G. Zhang and S. Pispas, *Macromolecules*, 2010, **43**, 1771–1777.
70 R. Plummer, D. J. T. Hill and A. K. Whittaker, *Macromolecules*, 2006, **39**, 8379–8388.
71 Y. Ma, W.-F. Dong, E. S. Kooij, M. A. Hempenius, H. Möhwald and G. J. Vancso, *Soft Matter*, 2007, **3**, 889–895.
72 G. Inzelt, *Electroanalytical Chemistry*, Marcel Dekker, Inc., New York, 1994, pp. 89–241.
73 E. C. Cho, Y. D. Kim and K. Cho, *Polymer*, 2004, **45**, 3195–3204.
74 S. Zou, M. A. Hempenius, H. Schönherr and G. J. Vancso, *Macromol. Rapid Commun.*, 2006, **27**, 103–108.
75 J. Xu and S. Liu, *J. Polym. Sci., Part A: Polym. Chem.*, 2008, **47**, 404–419.